SCIENCE CHINA
Life Sciences

THEMATIC ISSUE: Signaling and regulatory biology
• RESEARCH PAPER •

February 2017 Vol.60 No.2: 202–214
doi: 10.1007/s11427-016-0369-6

A novel synthetic small molecule YF-452 inhibits tumor growth through antiangiogenesis by suppressing VEGF receptor 2 signaling

Yongrui Liu[1†], Yuan He[1†], Feifei Yang[1], Xiaonan Cong[1], Jinhua Wang[1], Shihong Peng[1], Dan Gao[1], Weifang Wang[1], Liping Lan[1], Xuexiang Ying[2], Mingyao Liu[1,3], Yihua Chen[1*] & Zhengfang Yi[1**]

[1]*Shanghai Key Laboratory of Regulatory Biology, Institute of Biomedical Sciences and School of Life Sciences, East China Normal University, Shanghai 200241, China;*

[2]*Department of General Surgery, Shanghai Jiaotong University Affiliated Sixth People's Hospital, Shanghai 200000, China;*

[3]*Center for Cancer and Stem Cell Biology, Institute of Biosciences and Technology and Department of Molecular and Cellular Medicine, Texas A&M University Health Science Center, Houston 77030, USA*

Received November 30, 2016; accepted December 26, 2016

Tumor angiogenesis is characterized by abnormal vessel morphology, endowing tumor with highly hypoxia and unresponsive toward treatment. To date, mounting angiogenic factors have been discovered as therapeutic targets in antiangiogenic drug development. Among them, vascular endothelial growth factor receptor 2 (VEGFR2) inhibitors exerts potent antiangiogenic activity in tumor therapy. Therefore, it may provide a valid strategy for cancer treatment through targeting the tumor angiogenesis via VEGFR2 pathway. In this study, we established a high-profile compounds library and certificated a novel compound named *N*-(*N*-pyrrolidylacetyl)-9-(4-bromobenzyl)-1,3,4,9-tetrahydro-β-carboline (YF-452), which remarkably inhibited the migration, invasion and tube-like structure formation of human umbilical vein endothelial cells (HUVECs) with little toxicity *invitro*. Rat thoracic aorta ring assay indicated that YF-452 significantly blocked the formation of microvascular *exvivo*. In addition, YF-452 inhibited angiogenesis in chick chorioallantoic membrane (CAM) and mouse corneal micropocket assays. Moreover, YF-452 remarkably suppressed tumor growth in xenografts mice model. Furthermore, investigation of molecular mechanism revealed that YF-452 inhibited VEGF-induced phosphorylation of VEGFR2 kinase and the downstream protein kinases including extracellular signal regulated kinase (ERK), focal adhesion kinase (FAK) and Src. These results indicate that YF-452 inhibits angiogenesis and may be a potential antiangiogenic drug candidate for cancer therapy.

YF-452, angiogenesis, HUVECs, VEGFR2

Citation: Liu, Y., He, Y., Yang, F., Cong, X., Wang, J., Peng, S., Gao, D., Wang, W., Lan, L., Ying, X., Liu, M., Chen, Y., and Yi, Z. (2017). A novel synthetic small molecule YF-452 inhibits tumor growth through antiangiogenesis by suppressing VEGF receptor 2 signaling. Sci China Life Sci 60, 202–214. doi: 10.1007/s11427-016-0369-6

INTRODUCTION

Angiogenesis is a complex biological phenomenon of forming new blood vessels from the preexisting ones (Villanueva, 2015), and plays a critical role in tumor growth by supplying nutrients and oxygen, removing waste products from the tumor (Nagy and Dvorak, 2012). Thus, tumor angiogenesis has been thought as an attractive therapeutic target for combating cancer from the time of its recognition (Sitohy et al.,

†Contributed equally to the work
*Corresponding author (email: yhchen@bio.ecnu.edu.cn)
**Corresponding author (email: zfyi@bio.ecnu.edu.cn)

2012). Compared with chemotherapy directly targeting cancer cells which often mutate rapidly and acquire drug resistance to treatment, the antiangiogenic therapy is obviously advantageous with less toxicity and more selectivity (Liu et al., 2007).

Tumor angiogenesis is a multistep process regulated by numerous growth factors and cytokines. It is well known that vascular endothelial growth factor (VEGF) plays a pivotal role during angiogenic process (Shen et al., 2012), which is abundantly produced by hypoxic tumor cells, macrophages and other cells of immune system (Medici and Olsen, 2012). VEGF exerts its biological effect mainly via binding and activating vascular endothelial growth factor receptor 2 (VEGFR2), then regulating downstream signaling pathways. Activation of VEGFR2 leads to the stimulation of various downstream signals including extracellular signal regulated kinase (ERK), focal adhesion kinase (FAK), Src, phosphoinositide 3-kinase (PI3K), Akt (also known as protein kinase B) and so on (Cho et al., 2004; Qi and Claesson-Welsh, 2001; Schlessinger, 2000). The AKT signaling pathway regulates endothelial cell proliferation, migration and apoptosis (Jiang and Liu, 2008; Somanath et al., 2006). In addition, ERK1/2 activity is implicated in diverse cellular activities including cell proliferation, differentiation, migration and cell death (Berra et al., 2000; Pagès et al., 2000). Src phosphorylation has also been demonstrated to be a critical signaling mediator in the migration step of angiogenesis (Chung et al., 2010). Thus, VEGFR2 and those signaling mediators have been recognized as compelling targets for the suppression of angiogenesis. Currently, clinical trials focusing on the effect of antiangiogenic therapy are ongoing worldwide and there are increasing reports on antiangiogenic drugs utilized in clinical trials or still under clinical investigations (Capozzi et al., 2016; Zhao et al., 2016), consisting of macromolecular monoclonal antibodies targeting VEGF ligands or VEGFR2 as well as small molecular inhibitors suppressing kinase activity such as vandetanib and sunitinib (Fontanella et al., 2014; Pentheroudakis et al., 2014; Xu et al., 2011; Zhang et al., 2011; Zhu et al., 2013). Despite the spectacular progress made recently, most of angiogenesis inhibitors suffer some adverse effects in clinical uses or trials, such as hypertension, bleeding, proteinuria and gastrointestinal perforation, which cramps their chronic use (De Falco, 2014). Hence, discovering more novel antiangiogenic molecules as anticancer drug candidates is still imperatively needed at present.

In an effort to explore more potent angiogenesis inhibitors, we screened a series of compounds synthesized by our laboratory based on their inhibitory effects in HUVEC phenotypic assays and identified a novel small molecule compound named YF-452 as the most potent compound. The results *in vitro* revealed that YF-452 obviously inhibited HUVECs migration, invasion and tube formation without obvious cytotoxic effect. By using thoracic aorta ring assay, chick chorioallantoic membrane (CAM) assay and mouse corneal micropocket assay, we found that YF-452 blocked microvascular formation *ex vivo* and *in vivo*. Furthermore, YF-452 inhibited human prostate tumor growth by antagonizing tumor angiogenesis without obvious cytotoxic effect. In addition, we found that YF-452 exhibited antiangiogenic activity by blocking VEGF/VEGFR2 signaling pathway. Taken together, these results indicated that YF-452 may be a potential candidate in antiangiogenic therapy.

RESULTS

YF-452 inhibits HUVECs migration, invasion and tube formation with little toxicity

After screening sixty-two novel molecules from our laboratory compound library, nine small molecule compounds showed obvious inhibitory effect *in vitro* using wound healing assay (Figure S1 in Supporting Information). Among all the tested compounds, YF-452 exerted the most potent inhibition on HUVECs migration. The chemical structure of YF-452 was shown in Figure 1A.

To further determine the antiangiogenic activity of YF-452 *in vitro*, a wound healing assay was carried out for evaluating of its inhibitory effect on HUVECs migration (Figure S2 in Supporting Information). YF-452 remarkably inhibited the migration of endothelial cells in a concentration-dependent manner (Figure 1B). Transwell invasion assay was also conducted to measure the ability of HUVECs to pass through the membrane barrier of transwell. Compared with the control group, YF-452 caused significant inhibition of HUVECs invasion in a concentration-dependent manner (Figure 1C). In contrast to the two tyrosine receptor kinase inhibitors vandetanib and sunitinib, the invasion inhibition effect of YF-452 seemed comparable to vandetanib, which was slightly less than sunitinib (Figure S3 in Supporting Information).

The formation of capillaries from mature endothelial cells is the initial and prerequisite step in angiogenesis (Willmott and Monk, 2009). To detect whether YF-452 triggers antiangiogenic activity, VEGF-induced capillary tubule formation was performed and the result revealed YF-452 significantly interfered capillary-like tube formation of HUVECs on the surface of Matrigel (Figure 1D).

To evaluate if the inhibitory effect of cell migration, invasion and tube formation were caused by the cytotoxic effect, we performed flow cytometric annexin V-FITC/PI dual staining assay of HUVECs. No obvious apoptosis was detected when antivascular effects of YF-452 appearing (12 h) (Figure 1E). We also analyzed cell viability at different times of incubation by MTS assay. As shown in Figure 1F, cells were occurred a modest growth inhibition only after treated with YF-452 (10 μmol L^{-1}) for a longer time (24−48 h). No reduction of the viability was found when YF-452 suppressing HUVECs migration and tube formation (12 h). It seems YF-452

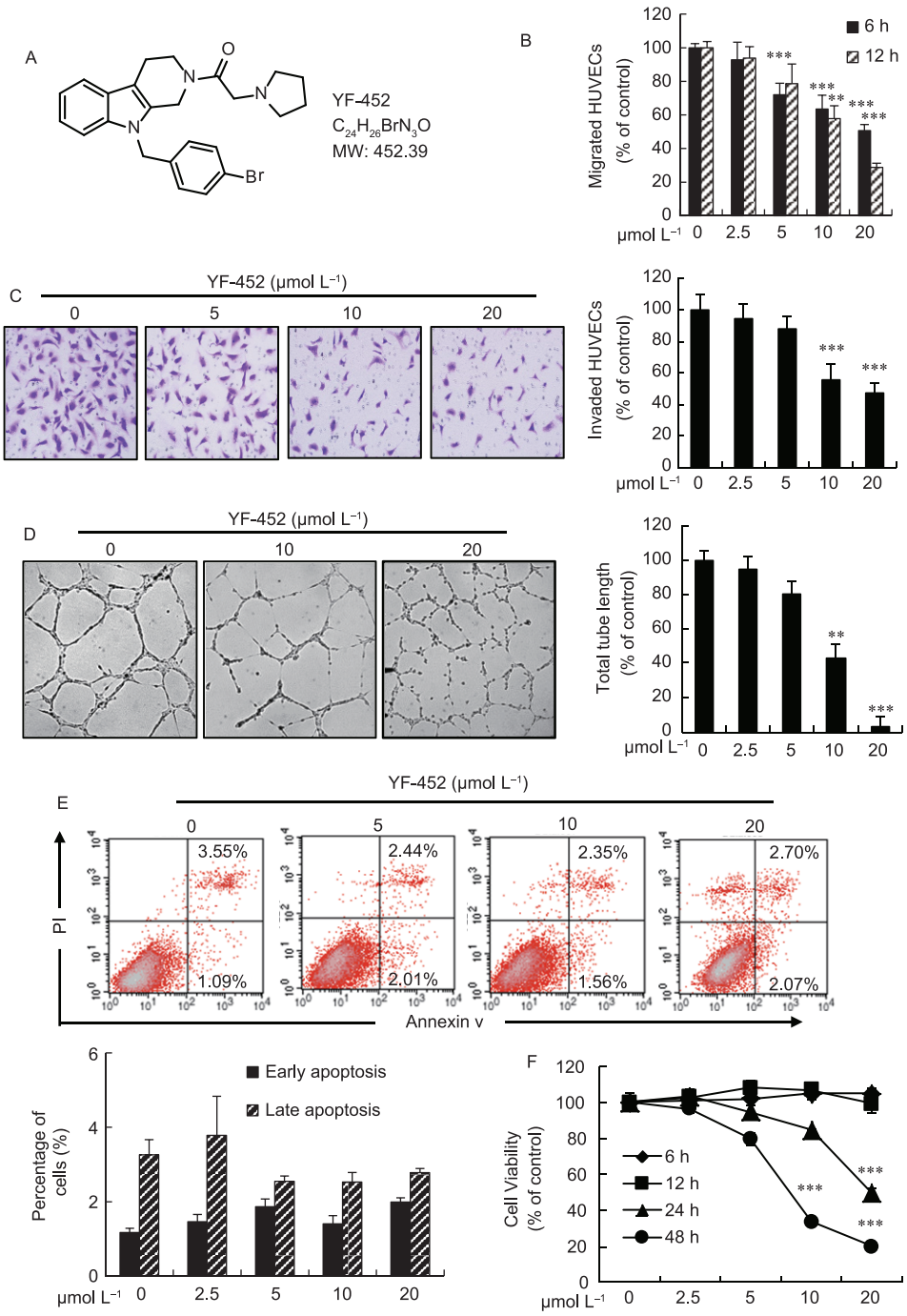

Figure 1 (Color online) Inhibitory effect on HUVECs migration, invasion and tube formation and toxicity evaluation of YF-452 *in vitro*. A, Chemical structure of YF-452. B, YF-452 inhibited HUVECs migration in wound healing assay. The cells were pretreated with mitomycin C to inhibit proliferation before inducing migration. Confluent HUVEC monolayers were scratch wounded and the cells were treated with indicated concentrations of YF-452 (0, 2.5, 5, 10, 20 μmol L^{-1}), then photographed at different times (6 or 12 h), and the migrated cells were quantified by manual counting. Technical replicates n=3. C, YF-452 inhibited HUVECs invasion in transwell assay. HUVECs were seeded in the top chamber and treated with different concentrations of YF-452. After 12 h, the cells that invaded through the membrane were stained and quantified. Technical replicates n=3. D, YF-452 inhibited capillary-like tube formation of HUVECs. After treated with indicated concentrations of YF-452 for 10 h, capillary-like structure in each group was quantified by IPP 6.0 software. The percentage of inhibition was expressed using control as 100%. Technical replicates n=3. E, HUVECs YF-452 treated for 12 h were assayed for apoptosis by flow cytometry using an annexin V-FITC/PI apoptosis detection kit. F, HUVECs were plated on 0.1% gelatin-coated 96 well plates and then treated with the indicated concentrations of YF-452. Cell viability at different time (6, 12, 24, 48 h) was determined by MTS assay. Technical replicates n=3. Error bars, SD. **, P<0.01; ***, P<0.001.

may not affect existing vasculature at the doses in antivascular assays we performed.

YF-452 inhibits angiogenesis *ex vivo* and *in vivo*

Prompted by the data *in vitro* supporting a potential antiangio-

genic activity of YF-452, we determined the effect of YF-452 on angiogenesis using rat thoracic aorta ring assay *ex vivo*, CAM assay and mouse corneal micropocket assay *in vivo*.

In rat thoracic aorta ring assay, as black arrows shown in Figure 2A, YF-452 obviously inhibited vessel sprouting from rat aortic rings in a concentration-dependent manner. The average area of sprouting vessels from thoracic aorta rings in the 10 μmol L^{-1} YF-452-treated group was decreased to only 10% of the control group. In order to further confirm the inhibitory effect of YF-452 on angiogenesis *in vivo*, we subsequently performed the CAM assay and mouse corneal micropocket assay, which were suitable and useful to discriminate cellular and behavioral aspects of angiogenesis (Schwartz et al., 2008). As shown in Figure 2B, in the area around the 5 mm diameter filter paper disk on the CAM of YF-452 groups, the formation of new blood vessels (indicated by arrows) was apparently reduced, suggesting YF-452 inhibiting angiogenesis in CAM assay. Similar inhibition effect of YF-452 appeared in mouse corneal micropocket assay. In the control group, VEGF (100 ng) obviously induced new blood vessels (Figure 2C, indicated by yellow arrows) to grow upwards to the pellet (Figure 2C, indicated by red arrows) from the corneoscleral limbus whereas the outgrowths were alleviated by YF-452 (10 and 20 μg) as indicated by clock number, new vessel length and vessel area (Figure 2C). During the whole experimentation, no symptoms of eye inflammation including keratitis, corneal edema and advanced signs of intraocular inflammation were observed (data not shown). These data reflected that YF-452 blocked VEGF-induced angiogenesis *ex vivo* and *in vivo*.

YF-452 inhibits PC-3 tumor xenograft growth

We next investigated the efficacy of YF-452 in tumor growth using a human prostate tumor xenograft mouse model. Nude mice bearing PC-3 tumors were intraperitoneal injected with YF-452 (20 and 40 mg kg^{-1} respectively) daily for 30 days, which obviously suppressed tumor size, tumor weight (Figure 3A) and tumor volume comparing with the vehicle group (Figure 3B).

To evaluate the health status of mice, weights of mice were monitored every 2 days throughout the whole experiment. No significant differences in weights were found among the three groups (Figure 3C). Similarly, we did not observe significant differences in the daily consumption of diet and drinking water among three groups, and no apparent physical signs of toxicity such as diarrhea, food and water withdrawal and impaired posture were appeared (data not shown). Furthermore, there were no toxic pathologic changes in hearts, livers, spleens, lungs, kidneys were detected in HE staining (Figure 3D). These data suggested the potential little side-effect of YF-452 at the therapeutic dosage, implying the inhibition of tumor growth was not attributable to systemic toxicity.

YF-452 inhibits tumor angiogenesis

When the experiment was terminated, all mice were sacrificed and the skin was peeled off to expose intact tumors, a marked decrease of intraneoplastic vascular density was observed in tumors from YF-452-treated mice versus control mice (Figure 4A, indicated by black arrows), supposing YF-452-mediated tumor growth suppression was closely related to angiogenesis inhibition.

To investigate the effect of YF-452 on angiogenesis in tumor, three tumors per group chosen at random were analyzed. The tumor microvasculature was visualized with the endothelial cell marker CD31 (PECAM-1) in immunofluorescence assay. Tumors from YF-452-treated mice had markedly lower microvessel abundance than the vehicle group, with CD31 signals reduced by more than 70% (Figure 4B, indicated by red arrows). These results demonstrated that YF-452 inhibited tumor growth by suppressing tumor angiogenesis.

YF-452 induces necrosis and apoptosis in tumor

The tumor histological changes in mice bearing PC-3 xenografts were observed by light microscopy after HE staining. As shown in Figure 4C, in the vehicle group tumor cells were densely packed, while in YF-452-treated groups tumor cells were sparse, and more necrotic regions appeared in tumor tissues.

Cell apoptosis from PC-3 tumors was evaluated via immunohistochemical assay for cleaved caspase-3. As black arrows indicated in Figure 4D, cleaved caspase-3 staining (the brown staining) was relatively increased in YF-452-treated groups compared with the vehicle group. Representative fields from each group were shown, the apoptotic cells in random fields from different tumors in each group were counted, and the apoptotic index is shown in Figure 4D. Furthermore, 20 μmol L^{-1} YF-452 significantly suppressed HUVECs proliferation without affecting PC-3 cells, while the inhibition effect of multi-targeted tyrosine kinase receptor inhibitors sunitinib and vandetanib exerted no significant cell selectivity between HUVEC and PC3 cells, indicating YF-452 were more sensitive to HUVECs than PC-3 cells (Figure S4 in Supporting Information). These results proposed a hypothesis that YF-452 provided less sufficient oxygen and nutrients, which concomitantly reduced neovascular growth and induced more tumor apoptosis instead of impacting PC-3 cells directly.

YF-452 inhibits VEGF/VEGFR2 signaling pathway

VEGFR2 plays a major role in tumor angiogenesis and previous studies indicated that blockage of VEGFR2 activity remarkably limits tumor angiogenesis process (Song et al., 2012). We examined the influence of YF-452 on phosphorylation of VEGFR2, the active form of VEGFR2 stimulated

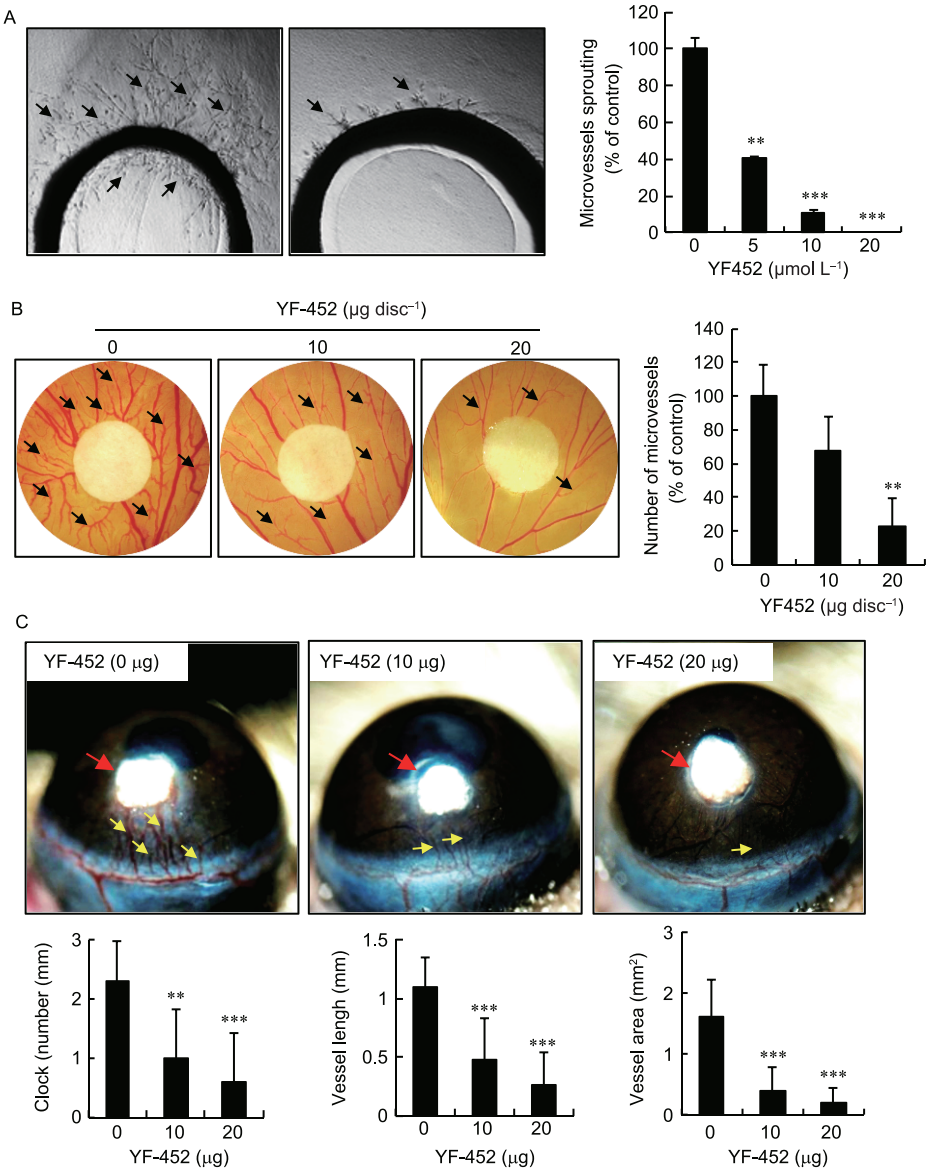

Figure 2 YF-452 inhibits angiogenesis *ex vivo* and *in vivo*. A, Representative images (left panel) and the optical density (right panel) of microvessels sprouting from rat thoracic aorta rings in the absence or presence of YF-452. The microvessel density of the untreated group was considered as 100%. Technical replicates $n=3$. B, YF-452 inhibited the formation of new blood vessels branches in CAM assay. Arrows pointed the new microvessels. Statistics indicated the percentage of inhibition and expressed using untreated group as 100%. Technical replicates $n=8$. C, YF-452 inhibited VEGF-induced angiogenesis in the mouse corneal micropocket assay. Red arrows pointed the micropellets and yellow arrows pointed VEGF-induced neovasculature. The statistical results showed the clock number, new vessel length and vessel area in each group. Images of both CAM and mouse corneal micropocket assays were obtained with OLYMPUS stereomicroscope. Technical replicates $n=8$. Error bars, SD. **, $P<0.01$; ***, $P<0.001$.

by VEGF. The expression of p-VEGFR2 (Tyr1175) and total VEGFR2 were assessed by western blotting assay in the presence of VEGF. As shown in Figure 5A, YF-452 inhibited VEGF-induced phosphorylation of VEGFR2 in a concentration-dependent manner, while the total level of VEGFR2 had limited changes.

VEGFR2 phosphorylation leads to the activation of various downstream signaling substrates that are responsible for endothelial cell migration and tube-like structure formation. To investigate the molecular mechanism of YF-452-mediated antiangiogenic properties, we screened some essential kinases involved in VEGFR2 signaling pathway. As shown in Figure 5A, YF-452 remarkably suppressed the activation of FAK, Src and ERK induced by VEGF, which indicated that YF-452 may inhibit angiogenesis through direct inhibition of VEGFR2 on the surface of endothelial cells. YF-452 was found to inhibit the phosphorylation of ERK1/2 and Src at the concentration of 5 μmol L^{-1} without affecting their total expression level. Furthermore, YF-452 also inhibited VEGF-induced phosphorylation of FAK at the dose of 10 and 20 μmol L^{-1}. While compared with HUVECs, PC-3 cells had a markedly lower expression of VEGFR2, which was not suf-

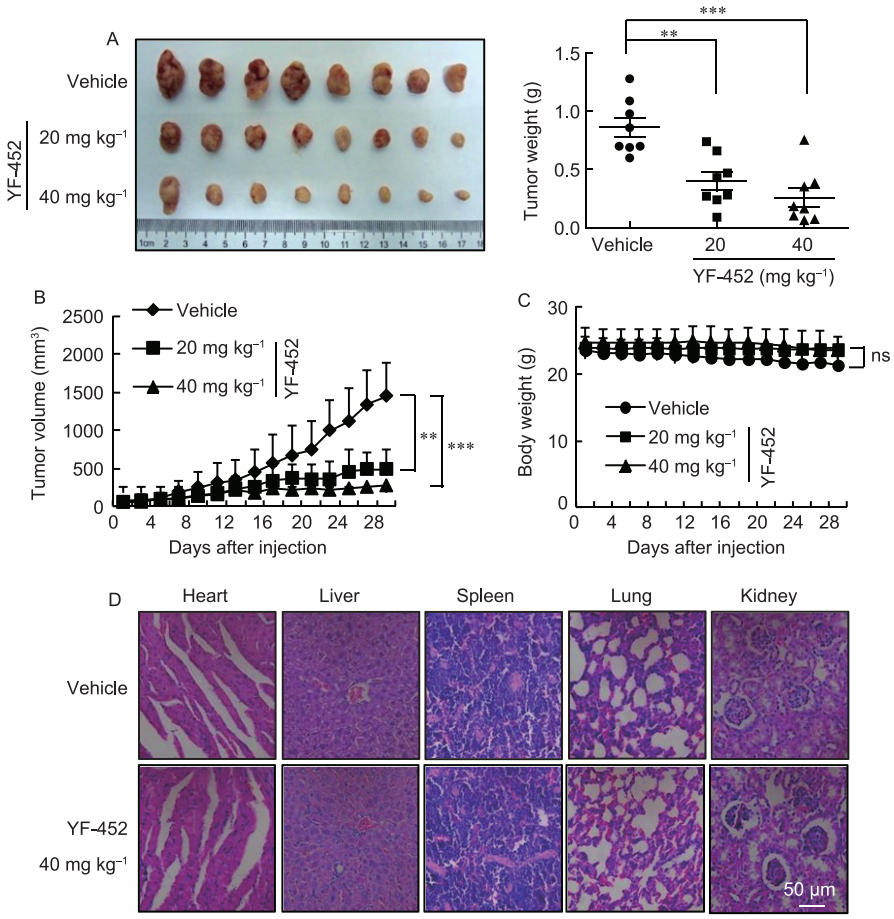

Figure 3 (Color online) Antitumor effect and toxicity evaluation of YF-452 *in vivo*. PC-3 tumor-bearing nude mice were treated as described with YF-452 at 20, 40 mg kg^{-1} or with vehicle. A, Compared with vehicle group, YF-452-treated groups showed significant inhibition of tumor growth. Technical replicates n=8. B, The treatment with YF-452 resulted in significant inhibition of tumor volume versus vehicle control. Technical replicates n=8. C, YF-452 did not cause obvious change of body weights. D, YF-452 did not cause obvious pathologic abnormalities in normal tissues. HE staining of paraffin-embedded sections of the hearts, livers, spleens, lungs and kidneys. Error bars, SD. **, P<0.01; ***, P<0.001.

ficient to activate various downstream signaling molecules for cell proliferation. Hence, to some extent, this well explained why YF-452 were more sensitive to HUVECs rather than PC-3 cells (Figure 5B). In order to verify whether the selectivity of YF-452 to HUVEC was derived from the high expression of VEGFR2, we transfected a pCMV3-His-KDR plasmid to overexpressed VEGFR2 in COS-7 cells, a cell line expressed undetectable VEGFR2 under normal condition. Concomitantly, cell selectivity of YF-452 to COS-7 cells reached the same level of HUVECs (Figure 5C), indicating the selectivity was tightly related to the high expression of VEGFR2. Taken together, our results demonstrated that YF-452 exerted its antiangiogenic effect by targeting VEGFR2 downstream certain signaling events.

DISSCUSSION

In this study, we have elucidated that a novel synthetic small molecule compound, YF-452, significantly inhibits angiogenesis *in vitro* and *in vivo* by blocking VEGFR2 pathway in endothelial cells.

Since the essential role of angiogenesis in tumor development and progression was first proposed by Judah Folkman (Folkman, 1971), the idea of antiangiogenesis as a therapeutic strategy has been accounted for several decades. Antiangiogenic therapy targeting endothelial cells offers advantages over therapies directly against tumor cells. For example, existing tumor blood vessels degradation cuts off the oxygen and nutrients needed for tumor rapid growth, concomitantly reducing the tumor blood vessels interstitial pressure and improving the chemotherapy drugs to transfer into the tumor tissue (Boehm et al., 1997; Huang, 2015). Angiogenesis is a hallmark of malignant cancers, and disruption of tumor vasculature is an active anticancer therapy (Jayson et al., 2016). In fact, several antiangiogenic therapies have been approved by Food and Drug Administration (FDA) for cancers, including the humanized antibody bevacizumab, the tyrosine kinase inhibitor sorafenib, vandetanib and sunitinib (Carmeliet and Jain, 2011; Jain, 2013; Wedge et al., 2002). Unfortunately, most current antiangiogenic drugs suffer some adverse effects

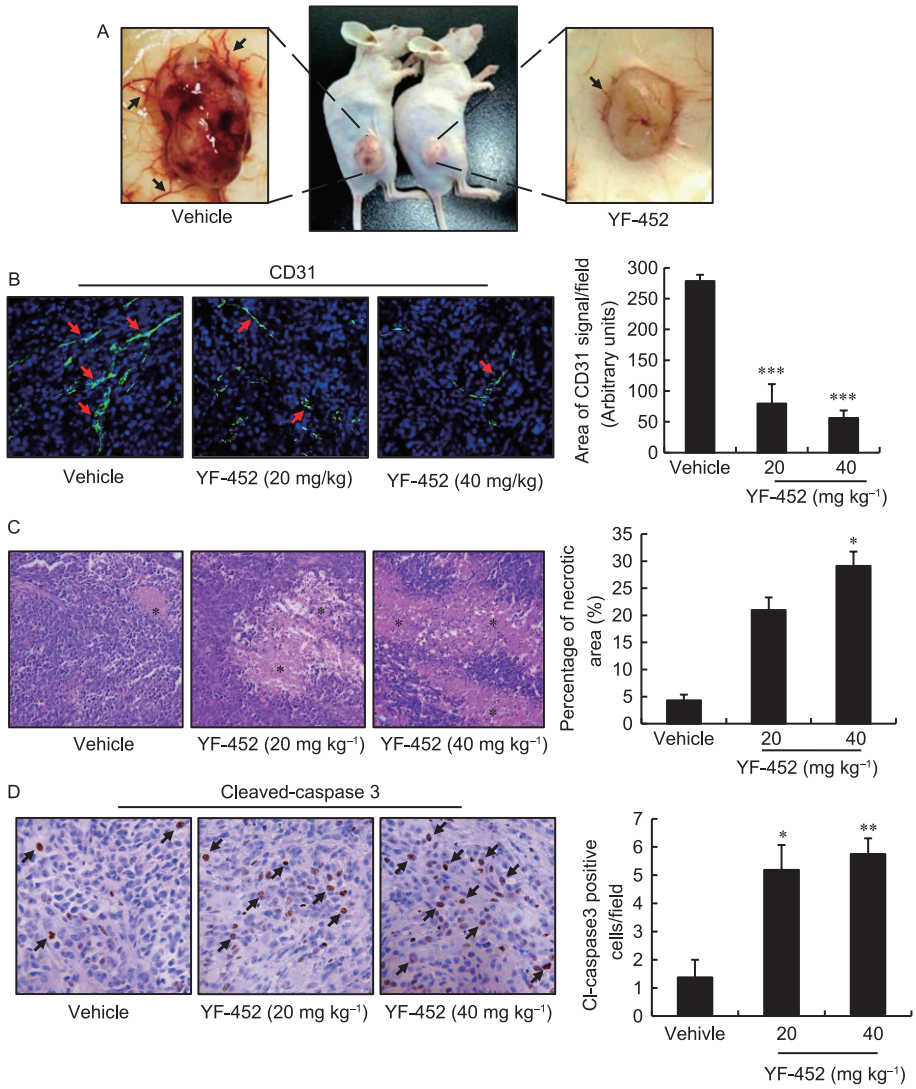

Figure 4 YF-452 inhibits tumor angiogenesis and induces necrosis as well as apoptosis in xenograft mouse model. A, YF-452 inhibited angiogenesis in tumor. B, CD31 staining was performed to indicate the blood vessels in tumor tissues. YF-452 apparently decreased CD31 fluorescent signal (green) in treated groups verse vehicle group. Nuclei were counterstained with 4′,6-diamidino-2-phenylindole (DAPI) (blue). Graph depicting CD31 immunofluorescence signal strengths in tumor tissues. C, Effect of YF-452 on the structural changes of tumors. Histopathological changes were observed under OLYMPUS stereomicroscope. Statistics indicated the percentage of necrotic areas per field (asterisks showed the necrotic tissue). D, Apoptosis was measured by cleaved caspase-3 staining in tumor sections. The treatment with YF-452 resulted in remarkably increased apoptosis versus vehicle control. Arrows indicated cleaved caspase-3 positive apoptotic cells. Statistics were calculated by cleaved caspase-3 positive cells/the total number of cells per field. Three random tumors were selected in three groups. Error bars, SD. *, $P<0.05$; **, $P<0.001$; ***, $P<0.001$.

and cause drug resistance in long-term therapy. Developing novel angiogenesis inhibitors as anticancer drug candidates is still in urgent need.

Therefore, we focus on the development of novel antiangiogenic compounds with low toxicity. According to the migration inhibitory effect of tested compounds to HUVECs listed in Figure S1 in Supporting Information, we analyzed that the structural framework played an important role in the anti-migration activities, overall the acylpyrrole compounds (YF-419, YF-375, YF-415, YF-417 and YF-339) showed poor inhibition on migration of HUVECs. However, among the indoles analogues, the Br-substitution on the phenyl accounted for the potential inhibitory activities (YF-361C vs. YF-420A). In addition, when the indole ring converted to tetrahydro-β-carboline, the compound became more potential (YF-452 vs. YF-420A). This result was explained by the surmise that carboline analogues targeted angiogenesis-related factor. Here, we demonstrate in detail that a novel synthetic small molecule compound, YF-452, exerts potent efficacy in inhibiting tumor angiogenesis.

In our study, YF-452 suppressed HUVECs migration and tube formation *in vitro* without significant toxicity (Figure 1), suggesting the presumption that YF-452 affected angiogenesis through targeting endothelial cells directly. In the research of angiogenesis, rat thoracic aorta ring assay and CAM assay are well established angiogenesis models (Dong et al., 2014).

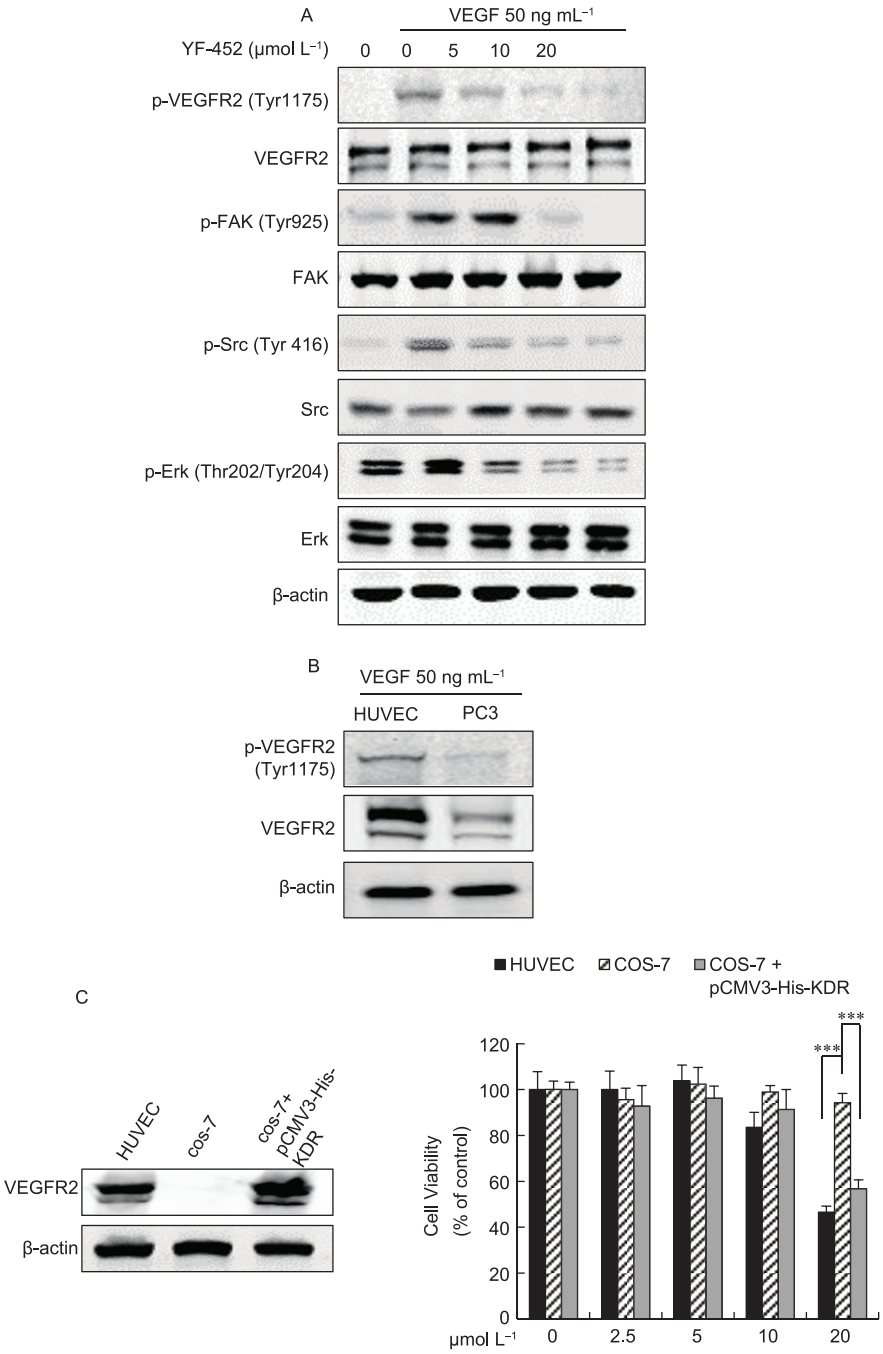

Figure 5 YF-452 inhibits the phosphorylation of VEGFR2 and its downstream signaling mediators. A, YF-452 suppressed the phosphorylation of VEGFR2 induced by VEGF in HUVECs. YF-452 also suppressed VEGFR2-mediated protein kinase activation of FAK, Src and ERK. B, To rule out YF-452 affecting tumor cells directly, expression of VEGFR2 and p-VEGFR2 were detected in HUVECs and PC-3 cells. Compared with HUVECs, a significantly lower expression of VEGFR2 in PC-3 cells was not sufficient to activate the phosphorylation of VEGFR2 and various downstream signaling molecules responsible for cell proliferation. C, The sensitivity of COS-7 cells to YF-452 was significantly increased after overexpression of VEGFR2. Error bars, SD. ***, $P<0.001$.

Moreover, the corneal micropocket assay is considered as the gold standard for evaluating angiogenesis *in vivo*. In all these angiogenesis models, YF-452 concentration-dependently suppressed the VEGF-induced proangiogenic effect (Figure 2). More importantly, YF-452 inhibited tumor growth by blocking angiogenesis with little side-effect in tumor xenograft model *in vivo* (Figure 3). Notably, YF-452 at the concentrations causing all these antiangiogenic effects induced slight influence on normal proliferation of endothelial cells, indicating existing normal vasculature in body would remain unaffected.

Our studies indicated that YF-452 was a potent inhibitor of angiogenesis by targeting VEGF/VEGFR2 signaling pathway (Figure 5A). VEGF and its high-affinity receptor VEGFR2 are the most widely studied factors in angiogenesis (Zhang et al., 2012). Thus targeting VEGFR-2 is an effective

strategy in the antiangiogenic therapy of tumors. Phosphorylation of VEGFR2 is critical for VEGF-mediated functions to vascular endothelial cells (Pober and Sessa, 2007; Zachary and Gliki, 2001). Tyr1175 is the main autophosphorylation site within VEGFR2, and its phosphorylation initiates the downstream signaling events in endothelial cells (Liu and Agarwal, 2010). Phosphorylated Tyr1175 of VEGFR2 mediates the activation of multiple downstream signaling components, including Src, which regulates vascular permeability and cell migration (Eliceiri et al., 2002; Takahashi et al., 2001). Then FAK and its substrate paxillin are involved in focal adhesion turnover during cell migration (Abedi and Zachary, 1997; Avraham et al., 2003; Holmqvist et al., 2004). In addition, ERK is also an important factor for regulating endothelial cell proliferation, growth, migration and apoptosis (Murphy et al., 2006). In the present study, YF-452 blocked the kinase activity of VEGFR2 definitely and showed an obvious decrease in the phosphorylation of FAK, Src and ERK, thus inhibited angiogenesis.

Albeit further studies are needed to reinforce these data, our studies, to a certain extent suggest that YF-452 suppresses angiogenesis by diminishing phosphorylation of VEGFR2. Further investigations are needed to explore the interacting proteins of YF-452. Meanwhile, its drug metabolism, pharmacokinetics and pharmacodynamics are also required more research, which help us evaluate YF-452 as a novel potential antiangiogenic drug in cancer therapy.

MATERIALS AND METHODS

Synthesis of YF-452

All commercially available starting reagents and materials were used without further purification. Nuclear Magnetic Resonance (NMR) spectra was recorded on a Bruker 300 or 500 MHz instrument and obtained as dimethyl sulfoxide-d6 (DMSO-d6) solutions (reported in ppm), using DMSO-d6 as the reference standard (2.50 ppm). Mass spectral data (ESI) was gathered on VG-7070 instrument.

As shown in Figure S5 in Supporting Information, the intermediate tetrahydro-β-carboline (1) was condensed with chloroacetyl chloride in tetrahydrofuran to yield *N*-chloroacetyl- 1,3,4,9-tetrahydro-β-carboline (2), which was condensed with pyrrolidine in DMF to yield compound *N*-pyrrolidylacetyl-1,3,4,9-tetrahydro-β-carboline (3), then converted to target compound YF-452 (yield=46.1%). ^{1}H NMR (DMSO, 300 MHz): δ 7.53−7.51 (m, 1H), 7.38 (d, *J*=8.4 Hz, 2H), 7.21 (dd, *J*=8.4, 8.4 Hz, 1H), 7.16−7.13 (m, 2H), 6.88 (d, *J*=8.4 Hz, 2H), 5.21 (s, 2H), 4.68 (s, 2H), 3.88 (t, *J*=6.6 Hz, 2H), 3.23 (s, 2H), 2.88 (t, *J*=6.6 Hz, 2H), 2.62−2.57 (m, 4H), 1.84−1.79 (m, 4H). (Synthesis route of YF-452 is available in Figure S5 in Supporting Information)

High performance liquid chromatography (HPLC) analysis of YF-452

HPLC (Agilent Technologies 1200 Series) was used for purification. The method showed as follow: Eclipse XDB C18 column, 5 μm, 4.6 mm×150 mm, column temperature 40°C; solvent A: water; solvent B: MeOH; gradient of 40%−90% B (0−10 min), 90% B (10−15 min), 90%−40% B (15−20 min); flow rate was 1.5 mL min^{-1}, injection volumes was 10 μL.

Preparation of YF-452

For all *in vitro* assays, YF-452 was prepared initially as 50 mmol L^{-1} stock solution in DMSO. Stock solution was diluted in the relevant assay media until indicated concentrations. For studies in CAM assay and mouse cornel micropocket assay, YF-452 was prepared as 4 and 40 mg mL^{-1} respectively and dosed at 5 μL disc^{-1} and 0.5 μL pellet^{-1}. For studies in nude mice, YF-452 was diluted in DMSO at 4 or 8 mg mL^{-1} and dosed at 0.1 mL 20 g^{-1} of body weight.

Cell lines, animals and reagents

Human prostate cancer cell line PC-3 and african green monkey kidney fibroblast cells COS-7 were obtained from American Type Culture Collection (ATCC) and cultured in RPMI-1640 and Dulbecco's Modified Eagle's Medium (DMEM) respectively (Gibco, USA). HUVECs were purchased from ATCC and cultured in completed endothelial cell medium (ECM) (ScienCell, USA).

All mediums were supplemented with 10% fetal bovine serum (Wisent). Fertilized chicken eggs were purchased from Shanghai Poultry Breeding Co. Ltd (Shanghai). C57BL/6 mice and male BALB/c nude mice were obtained from National Rodent Laboratory Animal Resources, Shanghai Branch of China. All animal experimental protocols were approved by the Animal Investigation Committee of the Institute of Biomedical Sciences, East China Normal University. Recombinant human VEGF ($VEGF_{165}$) was from R&D System (USA). Matrigel was purchased from BD Biosciences (USA). The pCMV3-His-KDR plasmid was purchased from Sino Biological Inc. (Beijing). Mitomycin C, Poly-hydroxyethyl methacrylate (poly-HEMA) and the antibody against β-actin were purchased from Sigma-Aldrich (USA). Antibodies for western blotting were purchased from Cell Signaling Technology (USA). The compound YF-452 was synthesized by our lab with the purity greater than 98%.

Cell viability assay

HUVEC and PC-3 cells were seeded in 96 well plates. After 12 h of incubation, cells were respectively treated with VEGF (10 ng mL^{-1}) and various concentrations of YF-452, vandetanib or sunitinib in fresh medium for 6 to 48 h. 20 μL Aqueous One solution (MTS; Promega, USA) per well was

added and spectrophotometric absorbance was measured at 490 nm using a microplate reader (SpectraMax 190; Molecular Devices, USA). The number of viable cells was presented relative to untreated control. This assay was repeated three times independently.

Wound healing assay

The wound healing assay was performed by plating cells in 6-well culture dishes (Goodwin, 2007). In brief, monolayer HUVECs were starved with basic ECM without FBS for 6 h and pretreated with mitomycin C for 2 h, then scratched with a pipette tip and washed with PBS. Fresh ECM medium without FBS containing different concentrations (0, 2.5, 5, 10, 20 μmol L^{-1}) of YF-452 and VEGF (10 ng mL^{-1}) was added to the scratched monolayer and incubated for 12 h. Images were taken using an OLYMPUS inverted microscope connected to a DXM1200 digital camera (Japan). The migrated cells were observed from three randomly selected fields and quantified by manual counting. Three independent experiments were performed.

Transwell invasion assay

Transwell invasion assay was performed in 24-well plates as previously described (Saraswati and Agrawal, 2013). HUVECs were trypsinized and seeded with 1×10^4 cells (100 μL) per well in medium with different concentrations of YF-452, vandetanib or sunitinib in upper chambers. The lower chambers were filled with 500 μL ECM medium containing VEGF (10 ng mL^{-1}) and the same concentrations of YF-452, vandetanib or sunitinib as upper chambers. After 12 h incubation at 37°C, non-invasive cells were scraped with a cotton swab, and invaded cells were fixed with 4% paraformaldehyde and stained with 0.1% crystal violet. Images were photographed using a digital camera attached to OLYMPUS inverted microscope, and invaded cells from three replicates were quantified by manual counting. Three independent experiments were performed.

Tube formation assay

Tube formation assay was conducted as previously described (Dong et al., 2010; Yan et al., 2015). 96-well plates were coated with 50 μL Matrigel per well and polymerized for 30 min at 37°C. HUVECs (1×10^4 cells) were suspended in ECM containing VEGF (10 ng mL^{-1}) and seeded on the Matrigel. Then they were treated with YF-452 of different concentrations. After 10 h, cells were photographed with a digital camera attached to OLYMPUS inverted microscope. Three independent experiments were performed.

Apoptosis assay

Cell apoptosis was analyzed by flow cytometry (FACS Calibur, BD, USA) as previously described (Dai et al., 2012). According to the manufacturer's instructions for the Annexin V-FITC/PI Apoptosis Detection Kit (BD Biosciences), HUVECs were treated with different concentrations (0, 2.5, 5, 10, 20 μmol L^{-1}) of YF-452 for 12 h. Then cells were trypsinized and harvested, washed with cold PBS and resuspended in 190 μL binding buffer with additional 5 μL annexin V and 5 μL propidium iodide (PI). The mixture was incubated for 15 min at room temperature avoiding light, then 400 μL binding buffer was added and cells were analyzed by flow cytometry (BD Biosciences) immediately. This assay was repeated three times independently.

Rat aortic ring assay

The *ex vivo* angiogenesis assay was performed as previously described (Dai et al., 2012). Thoracic aortas were removed from Sprague-Dawley rats (male; 8-week-old) and immediately transferred to a culture dish containing ice-cold serum-free MCDB131 media (Life Technologies Ltd, UK). The periaortic fibroadipose tissue around aortic wall was carefully removed with microdissecting forceps. Each aortic ring was sectioned and washed three times in MCDB131 media. 48-well plates were coated with 100 μL of Matrigel per well and polymerized at 37°C for 30 min. Ring-shaped explants of aorta were then plated in the wells and overlaid with 100 μL of Matrigel for sealing. After polymerization, VEGF (100 ng mL^{-1}) in serum-free MCDB131 culture medium, with or without 5, 10, 20 μmol L^{-1} YF-452 were added respectively. The rings were incubated at 37°C in a humidified environment for 7 days and the culture media was replaced every two days. The vascular sprouting was examined using a microscope equipped with a digital imaging system (OLYMPUS) and counted by Image-Pro 6.0 software.

Chick chorioallantoic membrane assay

Chick chorioallantoic membrane assay is operated as previously described (Dong et al., 2010). Embryonic eggs were incubated in 37°C with the relative humidity at 65%−70%. After 5 days, the eggs were equally divided into three groups and a 1 cm^2 window was opened at the blunt end of each egg and the shell membrane was removed slightly to expose the CAM. Then a sterilized 5 mm diameter filter paper disk (Whatman, USA) containing different concentrations of YF-452 or solvent control (DMSO) was placed on the CAM of each egg. The window was sealed and eggs were incubated for 48 h. New blood vessels were observed under a stereo-microscope and quantified using Image Pro Plus 6.0 software.

Mouse corneal micropocket assay

The *in vivo* anti-angiogenic activity of YF-452 was also assessed by a mouse corneal micropocket assay as previously described (Dong et al., 2010). Briefly, the slow-release pellets (0.35×0.35 mm^2) containing YF-452 and 100 ng $VEGF_{165}$ were prepared with sucrose octasulfate-aluminum

complex and poly-HEMA. A corneal micropocket was created in one eye of each 4-5-week-old C57BL/6 mouse, then the prepared pellet was implanted into the micropocket. Chlortetracycline hydrochloride ophthalmic ointment was applied to each operated eye to prevent infection. After 7 days, the vessel length and clock hours of new blood vessels were examined under a stereomicroscope and recorded. The area of neovasculature was calculated according to the formula: Area (mm^2)=0.2×3.14×VL(mm)×CN (mm), where the VL is the maximal vessel length extending from the limbal vasculature toward the pellet and CN is the clock hours of neovasculature, where one clock hour equals 30 degrees of arc.

Human prostate tumor xenograft mouse model

Five weeks old male BALB/c nude mice were purchased from National Rodent Laboratory Animal Resources (Shanghai). Animals were housed in a specific pathogen-free room within the animal facilities and were maintained in accordance with the current regulations and standards of the United States National Institutes of Health. All animals were allowed to acclimatize to their new environment for one week prior to use. Mice were randomly divided into three groups (8 mice $group^{-1}$). PC-3 cells (5×10^6 cells $mouse^{-1}$) were subcutaneously injected in the right sides of the dorsal area of the mice. When the tumors grew to about 50 mm^3, mice were injected intraperitoneally with DMSO or YF-452 (20 and 40 mg kg^{-1}) daily for 30 days. DMSO served as vehicle control. The body weight of each mice was recorded and tumor volume was measured with a digital vernier caliper every 2 days, following the formula of $0.52\times A\times B^2$, where A is the longest diameter and B is the shortest diameter of tumor (Lai et al., 2012). At the end of the experiment, mice were sacrificed and tumors were removed and processed for immunohistochemical analysis.

Toxicity evaluation

To investigate potential side-effect or toxicity on mice during treatment, mice of each group were monitored for relevant indexes including weight loss, diarrhea, food and water withdrawal and impaired posture. The tissues of hearts, livers, spleens, lungs and kidneys were stained with hematoxylin and eosin (Yang et al., 2014).

Histological analysis

Tumor tissues were fixed with 4% formaldehyde for 12 h, processed and embedded in paraffin blocks. The sections of lungs and other tissues were stained with hematoxylin and eosin. Histopathological changes were observed under a light microscope. Rat anti-mouse cleaved caspase-3 (Cell Signaling Technology, Catalog No. 9964) was used for immunohistochemistry to explore cell apoptosis in PC-3 tumors. Immuno-reactivity was visualized using peroxidase-diaminobenzidine (DAB) (Saraswati and Agrawal, 2013). Three tumors randomly chosen in each group were analyzed. The number of cleaved caspase-3-positive cells was quantified by Leica DM 4000B photomicroscope and the apoptotic index in six random fields per group was counted.

Detection of microvessel density (MVD)

The antiangiogenic activity of YF-452 was determined by frozen tumor sections immunofluorescence analysis (Tsoi et al., 2013). Tumor tissues were fixed in 4% formaldehyde for 4−6 h and processed with saccharose, embedded in optimal cutting temperature compound (Sakura Finetek USA, Inc.). Samples were stored at −80°C until they were sectioned and mounted on glass slides. The slides were thawed at room temperature for 20 min, permeabilized with 0.1% Triton X-100 in PBS for 30 min. Then the slides were blocked with 5% BSA diluted in PBS for 30 min, probed with rat anti-mouse CD31 antibody (1:100; Novus Biologicals NB100-2284) overnight at 4°C and washed with 1% Triton X-100 (Bioshop Canada, Inc., USA) in PBS for three times. The CD31 probed slides were incubated with the secondary antibody Alexa Fluor 488 goat anti-rat IgG (Catalog No. ZF-0511, dilution of 1:2000; Invitrogen, USA) for 1 h at room temperature in dark condition. The slides were washed with 0.1% Triton X-100 in PBS for 5 min repeating three times and mounted with VECTASHIELD Mounting Medium for fluorescence with DAPI (Vector Laboratories, Inc., USA). To evaluate the amount of CD31 signal, three tumors per group were chosen and five fields per tumor were selected at random and Image Pro Plus 6.0 software was used to quantify the area of signal emitted in each field.

Western blot analysis

HUVECs were serum-starved for 6 h and then washed with basic medium without serum. Followed by the stimulation with 50 ng mL^{-1} $VEGF_{165}$ in basic medium for 10 min as previously described (Pang et al., 2009), cells were treated with YF-452 (0, 5, 10, 20 μmol L^{-1}) in basic medium for 4 h. Cells were lysed with radioimmunoprecipitation assay (RIPA) buffer supplemented with phenylmethylsulfonyl fluoride (PMSF) and proteinase inhibitor cocktail (Sigma, USA). Protein concentrations were determined using BCA protein assay kit (Thermo Scientific, USA) and equalized before loading. 50 μg total cellular protein samples from each treated group were applied to 8% to 12% sodium dodecyl sulfate-polyacrylamide gel electrophoresis (SDS-PAGE) gels and transferred onto nitrocellulose membranes. Then membranes were blocked with 5% BSA in PBS and probed with specific primary antibodies (Cell Signaling Technology) including anti-β-actin (#4970), anti-VEGFR2 (#9698), anti-ERK1/2 (#4377), anti-Src (#2109), anti-FAK (#3285), anti-phospho-VEGFR2(Tyr1175) (#2479), anti-phospho-ERK1/2 (Thr202/Tyr204) (#4370), anti-phospho-Src

(Tyr416) (#2101), anti-phospho-FAK (Tyr925) (#3284) overnight in 4°C. Blots were incubated with florescence conjugated secondary antibodies and detected by the infrared dichroic laser scanning imaging system (Odyssey, Li-Cor, USA). Three independent experiments were performed.

Statistical analysis

The data were presented as mean±SD. Differences in the results were evaluated correspondingly using one-way ANOVA, two-way ANOVA or two-way repeated measures ANOVA. The significant differences of means were determined at the level of *, $P<0.05$, **, $P<0.01$ and ***, $P<0.001$. All experiments were performed at least three times except animal experiment.

Compliance and ethics *The author(s) declare that they have no conflict of interest. All procedures performed in studies involving animals were in accordance with the ethical standards of the animal investigation committee of the Institute of Biomedical Sciences, East China Normal University.*

Acknowledgements *This work was supported by Major State Basic Research Development Program of China (2015CB910400), National Natural Science Foundation of China (81272463, 81472788, 81330049, 81673304), and The Science and Technology Commission of Shanghai Municipality (15431902200).*

Abedi, H., and Zachary, I. (1997). Vascular endothelial growth factor stimulates tyrosine phosphorylation and recruitment to new focal adhesions of focal adhesion kinase and paxillin in endothelial cells. J Biol Chem 272, 15442–15451.

Avraham, H.K., Lee, T.H., Koh, Y., Kim, T.A., Jiang, S., Sussman, M., Samarel, A.M., and Avraham, S. (2003). Vascular endothelial growth factor regulates focal adhesion assembly in human brain microvascular endothelial cells through activation of the focal adhesion kinase and related adhesion focal tyrosine kinase. J Biol Chem 278, 36661–36668.

Berra, E., Milanini, J., Richard, D.E., Le Gall, M., Viñals, F., Gothié, E., Roux, D., Pagès, G., and Pouysségur, J. (2000). Signaling angiogenesis via p42/p44 MAP kinase and hypoxia. Biochem Pharmacol 60, 1171–1178.

Boehm, T., Folkman, J., Browder, T., and O'Reilly, M.S. (1997). Antiangiogenic therapy of experimental cancer does not induce acquired drug resistance. Nature 390, 404–407.

Capozzi, M., VON Arx, C., DE Divitiis, C., Ottaiano, A., Tatangelo, F., Romano, G.M., Tafuto, S., and Tafuto, S. (2016). Antiangiogenic therapy in pancreatic neuroendocrine tumors. Anticancer Res 36, 5025–5030.

Carmeliet, P., and Jain, R.K. (2011). Molecular mechanisms and clinical applications of angiogenesis. Nature 473, 298–307.

Cho, C.H., Lee, C.S., Chang, M., Jang, I.H., Kim, S.J., Hwang, I., Ryu, S.H., Lee, C.O., and Koh, G.Y. (2004). Localization of VEGFR-2 and PLD2 in endothelial caveolae is involved in VEGF-induced phosphorylation of MEK and ERK. Am J Physiol Heart Circ Physiol 286, H1881–H1888.

Chung, B.H., Cho, Y.L., Kim, J.D., Jo, H.S., Won, M.H., Lee, H., Ha, K.S., Kwon, Y.G., and Kim, Y.M. (2010). Promotion of direct angiogenesis *in vitro* and *in vivo* by *Puerariae flos* extract via activation of MEK/ERK-, PI3K/Akt/eNOS-, and Src/FAK-dependent pathways. Phytother Res 24, 934–940.

Dai, F., Chen, Y., Song, Y., Huang, L., Zhai, D., Dong, Y., Lai, L., Zhang, T., Li, D., Pang, X., Liu, M., and Yi, Z. (2012). A natural small molecule harmine inhibits angiogenesis and suppresses tumour growth through activation of p53 in endothelial cells. PLoS ONE 7, e52162.

De Falco, S. (2014). Antiangiogenesis therapy: an update after the first decade. Korean J Intern Med 29, 1–11.

Dong, Y., Lu, B., Zhang, X., Zhang, J., Lai, L., Li, D., Wu, Y., Song, Y., Luo, J., Pang, X., Yi, Z., and Liu, M. (2010). Cucurbitacin E, a tetracyclic triterpenes compound from Chinese medicine, inhibits tumor angiogenesis through VEGFR2-mediated Jak2-STAT3 signaling pathway. Carcinogenesis 31, 2097–2104.

Dong, Y., Zhang, T., Li, J., Deng, H., Song, Y., Zhai, D., Peng, Y., Lu, X., Liu, M., Zhao, Y., and Yi, Z. (2014). Oridonin inhibits tumor growth and metastasis through anti-angiogenesis by blocking the notch signaling. PLoS ONE 9, e113830.

Eliceiri, B.P., Puente, X.S., Hood, J.D., Stupack, D.G., Schlaepfer, D.D., Huang, X.Z., Sheppard, D., and Cheresh, D.A. (2002). Src-mediated coupling of focal adhesion kinase to integrin αvβ5 in vascular endothelial growth factor signaling. J Cell Biol 157, 149–160.

Folkman, J. (1971). Tumor angiogenesis: therapeutic implications. N Engl J Med 285, 1182–1186.

Fontanella, C., Ongaro, E., Bolzonello, S., Guardascione, M., Fasola, G., and Aprile, G. (2014). Clinical advances in the development of novel VEGFR2 inhibitors. Ann Transl Med 2, 123.

Goodwin, A.M. (2007). *In vitro* assays of angiogenesis for assessment of angiogenic and anti-angiogenic agents. Microvasc Res 74, 172–183.

Holmqvist, K., Cross, M.J., Rolny, C., Hägerkvist, R., Rahimi, N., Matsumoto, T., Claesson-Welsh, L., and Welsh, M. (2004). The adaptor protein Shb binds to tyrosine 1175 in vascular endothelial growth factor (VEGF) receptor-2 and regulates VEGF-dependent cellular migration. J Biol Chem 279, 22267–22275.

Huang, B. (2015). Tumor microenvironment: a mechanical force link. Sci China Life Sci 58, 202–204.

Jain, R.K. (2013). Normalizing tumor microenvironment to treat cancer: bench to bedside to biomarkers. J Clin Oncol 31, 2205–2218.

Jayson, G.C., Kerbel, R., Ellis, L.M., and Harris, A.L. (2016). Antiangiogenic therapy in oncology: current status and future directions. Lancet 388, 518–529.

Jiang, B.H., and Liu, L.Z. (2008). AKT signaling in regulating angiogenesis. Curr Cancer Drug Targets 8, 19–26.

Lai, L., Liu, J., Zhai, D., Lin, Q., He, L., Dong, Y., Zhang, J., Lu, B., Chen, Y., Yi, Z., and Liu, M. (2012). Plumbagin inhibits tumour angiogenesis and tumour growth through the Ras signalling pathway following activation of the VEGF receptor-2. British J Pharmacol 165, 1084–1096.

Liu, F., Tan, G., Li, J., Dong, X., Krissansen, G.W., and Sun, X. (2007). Gene transfer of endostatin enhances the efficacy of doxorubicin to suppress human hepatocellular carcinomas in mice. Cancer Sci 98, 1381–1387.

Liu, J., and Agarwal, S. (2010). Mechanical signals activate vascular endothelial growth factor receptor-2 to upregulate endothelial cell proliferation during inflammation. J Immunol 185, 1215–1221.

Medici, D., and Olsen, B.R. (2012). Rapamycin inhibits proliferation of hemangioma endothelial cells by reducing HIF-1-dependent expression of VEGF. PLoS ONE 7, e42913.

Murphy, D.A., Makonnen, S., Lassoued, W., Feldman, M.D., Carter, C., and Lee, W.M.F. (2006). Inhibition of tumor endothelial ERK activation, angiogenesis, and tumor growth by sorafenib (BAY43-9006). Am J Pathol 169, 1875–1885.

Nagy, J.A., and Dvorak, H.F. (2012). Heterogeneity of the tumor vasculature: the need for new tumor blood vessel type-specific targets. Clin Exp Metastasis 29, 657–662.

Pagès, G., Milanini, J., Richard, D.E., Berra, E., GothiÉ, E., Viñals, F., and PouyssÉGur, J. (2000). Signaling angiogenesis via p42/p44 MAP kinase cascade. Ann New York Acad Sci 902, 187–200.

Pang, X., Yi, Z., Zhang, X., Sung, B., Qu, W., Lian, X., Aggarwal, B.B., and Liu, M. (2009). Acetyl-11-keto-β-boswellic acid inhibits prostate tumor growth by suppressing vascular endothelial growth factor receptor 2-mediated angiogenesis. Cancer Res 69, 5893–5900.

Pentheroudakis, G., Kotoula, V., Kouvatseas, G., Charalambous, E., Dionysopoulos, D., Zagouri, F., Koutras, A., Papazisis, K., Pectasides, D., Samantas, E., Dimopoulos, M.A., Papandreou, C.N., and Fountzilas,

G. (2014). Association of VEGF-A splice variant mRNA expression with outcome in bevacizumab-treated patients with metastatic breast cancer. Clin Breast Cancer 14, 330–338.
Pober, J.S., and Sessa, W.C. (2007). Evolving functions of endothelial cells in inflammation. Nat Rev Immunol 7, 803–815.
Qi, J.H., and Claesson-Welsh, L. (2001). VEGF-induced activation of phosphoinositide 3-kinase is dependent on focal adhesion kinase. Exp Cell Res 263, 173–182.
Saraswati, S., and Agrawal, S.S. (2013). Brucine, an indole alkaloid from Strychnos nux-vomica attenuates VEGF-induced angiogenesis via inhibiting VEGFR2 signaling pathway *in vitro* and *in vivo*. Cancer Lett 332, 83–93.
Schlessinger, J. (2000). New roles for src kinases in control of cell survival and angiogenesis. Cell 100, 293–296.
Schwartz, S., George, J., Ben-Shoshan, J., Luboshits, G., Avni, I., Levkovitch-Verbin, H., Ziv, H., Rosner, M., and Barak, A. (2008). Drug modification of angiogenesis in a rat cornea model. Invest Ophthalmol Vis Sci 49, 250.
Shen, K., Ji, L., Gong, C., Ma, Y., Yang, L., Fan, Y., Hou, M., and Wang, Z. (2012). Notoginsenoside Ft1 promotes angiogenesis via HIF-1α mediated VEGF secretion and the regulation of PI3K/AKT and Raf/MEK/ERK signaling pathways. Biochem Pharmacol 84, 784–792.
Sitohy, B., Nagy, J.A., and Dvorak, H.F. (2012). Anti-VEGF/VEGFR therapy for cancer: reassessing the target. Cancer Res 72, 1909–1914.
Somanath, P.R., Razorenova, O.V., Chen, J., and Byzova, T.V. (2006). Akt1 in endothelial cell and angiogenesis. Cell Cycle 5, 512–518.
Song, Y., Dai, F., Zhai, D., Dong, Y., Zhang, J., Lu, B., Luo, J., Liu, M., and Yi, Z. (2012). Usnic acid inhibits breast tumor angiogenesis and growth by suppressing VEGFR2-mediated AKT and ERK1/2 signaling pathways. Angiogenesis 15, 421–432.
Takahashi, T., Yamaguchi, S., Chida, K., and Shibuya, M. (2001). A single autophosphorylation site on KDR/Flk-1 is essential for VEGF-A-dependent activation of PLC-gamma and DNA synthesis in vascular endothelial cells. EMBO J 20, 2768–2778.
Tsoi, M., Laguëëlle, M.N., Boyer, A., Paquet, M., Nadeau, M.È., and Boerboom, D. (2013). Anti-VEGFA therapy reduces tumor growth and extends survival in a murine model of ovarian granulosa cell tumor. Transl Oncol 6, 226–IN1.
Villanueva, M.T. (2015). Angiogenesis: a sudden rush of blood to the tumour. Nat Rev Cancer 15, 135–135.
Wedge, S.R., Ogilvie, D.J., Dukes, M., Kendrew, J., Chester, R., Jackson, J.A., Boffey, S.J., Valentine, P.J., Curwen, J.O., Musgrove, H.L., Graham, G.A., Hughes, G.D., Thomas, A.P., Stokes, E.S., Curry, B., Richmond, G.H., Wadsworth, P.F., Bigley, A.L., and Hennequin, L.F. (2002). ZD6474 inhibits vascular endothelial growth factor signaling, angiogenesis, and tumor growth following oral administration. Cancer Res 62, 4645–4655.
Willmott, L.J., and Monk, B.J. (2009). Cervical cancer therapy: current, future and anti-angiogensis targeted treatment. Expert Rev Anticancer Therapy 9, 895–903.
Xu, D., Wang, T.L., Sun, L.P., and You, Q.D. (2011). Recent progress of small molecular VEGFR inhibitors as anticancer agents. Mini Rev Med Chem 11, 18–31.
Yan, X.C., Yang, Z.Y., Chen, Y., Li, N., Wang, L., Dou, G.R., Liu, Y., Duan, J.L., Feng, L., Deng, S.M., Han, H., and Zhang, P. (2015). Endothelial cells-targeted soluble human Delta-like 4 suppresses both physiological and pathological ocular angiogenesis. Sci China Life Sci 58, 425–431.
Yang, J.H., Hu, J., Wan, L., and Chen, L.J. (2014). Barbigerone inhibits tumor angiogenesis, growth and metastasis in melanoma. Asian Pac J Cancer Prev 15, 167–174.
Zachary, I., and Gliki, G. (2001). Signaling transduction mechanisms mediating biological actions of the vascular endothelial growth factor family. Cardiovasc Res 49, 568–581.
Zhang, S., Cao, Z., Tian, H., Shen, G., Ma, Y., Xie, H., Liu, Y., Zhao, C., Deng, S., Yang, Y., Zheng, R., Li, W., Zhang, N., Liu, S., Wang, W., Dai, L., Shi, S., Cheng, L., Pan, Y., Feng, S., Zhao, X., Deng, H., Yang, S., and Wei, Y. (2011). SKLB1002, a novel potent inhibitor of VEGF receptor 2 signaling, inhibits angiogenesis and tumor growth *in vivo*. Clin Cancer Res 17, 4439–4450.
Zhang, Y.M., Dai, B.L., Zheng, L., Zhan, Y.Z., Zhang, J., Smith, W.W., Wang, X.L., Chen, Y.N., and He, L.C. (2012). A novel angiogenesis inhibitor impairs lovo cell survival via targeting against human VEGFR and its signaling pathway of phosphorylation. Cell Death Dis 3, e406.
Zhao, X., Su, Y., You, J., Gong, L., Zhang, Z., Wang, M., Zhao, Z., Zhang, Z., Li, X., and Wang, C. (2016). Combining antiangiogenic therapy with neoadjuvant chemotherapy increases treatment efficacy in stage IIIA (N2) non-small cell lung cancer without increasing adverse effects. Oncotarget 7, 62619–62626.
Zhu, A.X., Finn, R.S., Mulcahy, M., Gurtler, J., Sun, W., Schwartz, J.D., Dalal, R.P., Joshi, A., Hozak, R.R., Xu, Y., Ancukiewicz, M., Jain, R.K., Nugent, F.W., Duda, D.G., and Stuart, K. (2013). A phase II and biomarker study of ramucirumab, a human monoclonal antibody targeting the VEGF receptor-2, as first-line monotherapy in patients with advanced hepatocellular cancer. Clin Cancer Res 19, 6614–6623.

SUPPORTING INFORMATION

Figure S1 Migration inhibitory rate of selected nine compounds on HUVECs.

Figure S2 YF-452 concentration and time dependently suppressed HUVECs migration.

Figure S3 Vandetanib and sunitinib concentration dependently suppressed HUVECs invision.

Figure S4 Compared with vandetanib and sunitinib, YF-452 showed a better selectivity on HUVEC than PC-3 cells in MTS assay.

Figure S5 The synthesis route of small molecule compounds YF-452.

The supporting information is available online at life.scichina.com and www.springerlink.com. The supporting materials are published as submitted, without typesetting or editing. The responsibility for scientific accuracy and content remains entirely with the authors.